Green's functions for antiferromagnetic polaritons. II. Scattering from rough surfaces

R. L. Stamps
Department of Physics, Colorado State University, Fort Collins, Colorado 80523

R. E. Camley
Department of Physics, University of Colorado, Colorado Springs, Colorado 80933
(Received 29 July 1988)

The scattering of an incident electromagnetic wave from a semi-infinite antiferromagnet with a rough surface is treated using the classical Maxwell wave equations. We limit our discussion to scattering within polarizations perpendicular to the plane of incidence. We first calculate the roughness-induced scattering from a periodic grating and show how the grating can couple the incident wave to both the forward ($+k_x$) and backward ($-k_x$) traveling surface-polariton states. We also find that the grating can induce strong coupling to the Brewster-type "leaky" modes. Finally we consider scattering from a randomly varying surface and estimate the change in reflectivity due to roughness-induced scattering into surface-polariton states.

I. INTRODUCTION

Interest in the effects of surface roughness on surface polaritons stems from a number of considerations. Foremost, of course, is the fact that roughness is always present in reality, no matter how perfect a sample may be, and necessarily influences any optical measurement of the material. In addition, roughness may increase coupling of electromagnetic waves to the normal modes of a material (particularly the surface modes), as with photons to plasmon-polaritons in a rough metal,[1] by causing the photon of wave vector $\mathbf{k}$ and frequency ω to interact with polariton modes also of frequency ω but with wave vectors in a range determined by the roughness. The presence of roughness yields a width in wavelength for the response of the media to driving fields analogous to the way dissipation mechanisms result in a width in frequency. Hence surface roughness plays a role determining the linewidths of absorption and scattering spectra.[2] Furthermore, since surface polaritons exist on the interface between two media, surface roughness clearly plays an important role in the excitation and propagation of surface polaritons by affecting the geometry of the interface.

Surface roughness provides two mechanisms by which surface polaritons can lose energy: either through roughness induced radiation or through roughness induced scattering into different polariton states. Which mechanism dominates depends on the polariton's frequency. Thus surface roughness can affect the mean free path length of polaritons propagating on the surface of a material. These mechanisms have in fact been suggested as explanations of certain anomalies in attenuated total reflection measurements of plasmon-polaritons.[3] Another effect due to random roughness is the shifting of frequencies of surface-polariton states below their flat surface frequencies, thus displacing the dips in reflectivity curves by amounts dependent on the distribution of heights and profiles that characterize the roughness.[4] Again, this is also a typical consequence of dissipation mechanisms.

For periodic gratings, a number of interesting results also appear. The effect of a grating is to couple the incident electromagnetic wave, with wave vector k_{xo} parallel to the surface, with polariton modes at wave vectors $k_{xo}+g$ where g is a reciprocal lattice vector for the periodic grating. This is a discrete form of the wavelength smearing described for random roughness. This process is analogous to the scattering of electrons in periodic potentials, and one can construct reduced Brillouin zone representations for the surface-polariton modes.[5] Other features reminiscent of energy bands is the appearance of "band gaps" in the surface-polariton dispersion relations that exist at the Brillouin zone boundaries.[3] Finally, we note that it is also possible that the fields very near a rough surface are enhanced to such a degree as to significantly affect nonlinear optical processes.[6]

Numerous theoretical methods have been developed which attempt to describe the effects of various types of surface roughness. Scattering due to random roughness has been treated by perturbation methods in the limit of small surface height fluctuations using a variety of classical formulations. Earlier methods[7,8] expanded the fields and surface profiles in power series under the assumption of small fluctuations in surface heights. Later formulations considered perturbations in the dielectric functions due to surface roughness and solved integral equations in the manner of the Born approximation of scattering theory.[1,2] Microscopic quantum-mechanical approaches have also been implemented, and the resulting expressions for scattering cross sections have been shown consistent with the classical perturbation theories.[9]

The above approaches all suffer from the assumption of roughness profiles that are small with respect to the wavelength of the incident light. These perturbative techniques are usually only carried to first order and sub-

sequently do not describe many of the more interesting features found in large amplitude studies (band gaps, frequency shifts, etc.). Alternative approaches have also been developed which attempt to deal with large amplitude gratings, and these constitute a whole subject unto themselves. Most notable are formulations of the Rayleigh hypothesis, which assumes that fields inside and outside the surface, or selvedge, region are also valid inside the selvedge region and may be used to satisfy the appropriate boundary conditions at the surface. Another technique is an integral equation method based on the "extinction theorem" which allows a formally exact solution for the scattered fields in all regions without invoking the Rayleigh assumption.[10] Each method has its disadvantages, the Rayleigh hypothesis being limited to describing fields in regions outside the surface region and the extinction theorem being difficult to implement numerically. Consequently, new techniques are constantly evolving.

Mindful of the above remarks, our aim in this paper is to provide a preliminary study of the effects of surface roughness on light scattering from semi-infinite uniaxial antiferromagnets. Most of the previous studies have considered the effects of roughness on only plasmon-polaritons and ferromagnetic magnons.[11] We will be most concerned with the scattering of light near antiferromagnetic surface-polariton frequencies, where the scattered light's amplitude and linewidth are related to the total magnitude of the power scattered into surface-polariton states.

We will assume the roughness is slight and follow the perturbation method used by Mills and Maradudin in their initial studies of scattering from rough metals.[1-4] This method, though not without certain shortcomings, provides a reasonable first attack on the problem and can be shown to be consistent with other techniques, at least to first order in the roughness height.[10,12] Since this technique requires the Green's functions for a semi-infinite antiferromagnet, we refer to the preceding paper (paper I) of this present work (paper II) for the derivation of these functions.

Once expressions for the roughness induced scattered fields are obtained, we then estimate the power losses due to roughness from a beam specularly reflected by the surface of an antiferromagnet. Since random roughness can be considered as a superposition of random periodic gratings of varying height, we will first consider the case of a sinusoidal one-dimensional grating impressed upon the material's surface. From there we will represent the randomly rough surface as an average of surface profiles, as also done by Mills and Maradudin,[1] with a Gaussian distribution of surface heights and profiles.

Besides allowing an incident beam to couple with either or both the $+k$ and the $-k$ surface-polariton branches, we also find that surface roughness can *enhance* the nonreciprocal reflectivity of an antiferromagnet in an applied field. In other words, in an applied field we find that the difference in reflectivity between a beam incident at $+\theta$ and a beam incident at $-\theta$, both of which couple to the surface-polariton modes, is increased by the presence of random roughness. We also find the interesting result that roughness allows coupling between an incident beam and the Brewster-type modes of a damped antiferromagnet. The properties of these damped modes are discussed in detail in paper I.

The outline of the present paper is as follows: in Sec. II we derive the integral equation for the scattered fields and solve for the power flow inside and outside the material. In Sec. III we study the effects of a small amplitude periodic grating on coupling with surface polaritons on MnF_2. Finally, in Sec. IV we consider the case of random surface roughness.

II. THEORY

The geometry is shown in Fig. 1. The material is in the $y > 0$ half-space and the surface varies about the xz plane. The antiferromagnet is assumed to be uniaxial and the magnetizations of the two sublattices are taken along the $\pm z$ axes. The applied field is also set along $\hat{z}$. The actual surface height is some function $\zeta(x,z)$ which measures the deviation of the actual surface above an ideal smooth surface at $y = 0$.

The dielectric properties of the material are determined by the dielectric tensor. For a uniaxial antiferromagnet this tensor is diagonal but anisotropic. The magnetic susceptibility has off diagonal elements in the presence of an applied field, and is also anisotropic. The explicit forms are given in paper I by Eq. (2.1)–(2.7), and in keeping with the notation of paper I, these are labeled $\overleftrightarrow{\epsilon}$ and $\overleftrightarrow{\mu}$.

The electric and magnetic susceptibilities are uniform everywhere except near the surface of the material. The only x and z dependence of the susceptibilities enters through the profile function $\zeta(x,z)$. Assuming a wavelength region where a step function behavior of the sus-

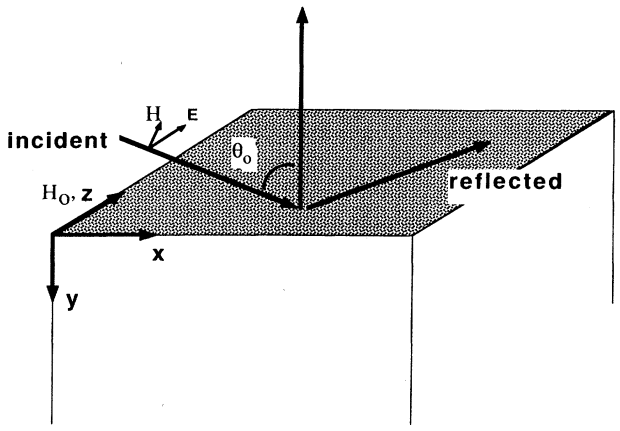

FIG. 1. Geometry for this paper. An electromagnetic wave with its electric field along z and H field in the xy plane is incident on an antiferromagnet with a rough surface. The material lies in the $y > 0$ half space with the easy axis along z. An applied field is also set along the z axis. The angle of incidence θ_0 is defined between the incident wave vector and the outward normal from the surface of the antiferromagnet.

ceptibilities at the surface is appropriate, we write the dependence of the susceptibilities on the roughness profile $\zeta(x,z)$ through the step function $\Theta(\zeta(x,z)-y)$:

$$\epsilon_{ij}^{r}(\mathbf{x})=\epsilon_{ij}+(\delta_{ij}-\epsilon_{ij})\Theta(\zeta(x,z)-y)\ , \tag{2.1}$$

$$\mu_{ij}^{r}(\mathbf{x})=\mu_{ij}+(\delta_{ij}-\mu_{ij})\Theta(\zeta(x,z)-y)\ . \tag{2.2}$$

Here δ_{ij} is the kronecker delta function which makes the dielectric and magnetic susceptibility tensors equal to unit matrices for the vacuum region. Note that we have written the susceptibilities as tensor components. The r superscripts denote the position-dependent functions for the geometry of a rough surface and the unsubscripted ϵ_{ij} and μ_{ij} are the components of $\overleftrightarrow{\epsilon}$ and $\overleftrightarrow{\mu}$.

The roughness is treated as a small perturbation in the susceptibilities. The position dependent rough surface susceptibility tensors $\overleftrightarrow{\epsilon}^{r}$ and $\overleftrightarrow{\mu}^{r}$ are expanded to first order in the perturbation as

$$\overleftrightarrow{\epsilon}^{r}=\overleftrightarrow{\epsilon}^{f}+\delta\overleftrightarrow{\epsilon}\ , \tag{2.3}$$

$$\overleftrightarrow{\mu}^{r}=\overleftrightarrow{\mu}^{f}+\delta\overleftrightarrow{\mu}\ , \tag{2.4}$$

where the flat surface susceptibilities $\overleftrightarrow{\epsilon}^{f}$ and $\overleftrightarrow{\mu}^{f}$ have components $\epsilon_{ij}+(\delta_{ij}-\epsilon_{ij})\Theta(-y)$ and $\mu_{ij}+(\delta_{ij}-\mu_{ij})\Theta(-y)$, respectively.

Expressions of this form can be found by expanding the susceptibilities in (2.1) and (2.2) in a Taylor's series about $\zeta(x,z)=0$. The first-order terms appearing in this expansion are

$$\delta\epsilon_{ij}=\zeta(x,z)(\delta_{ij}-\epsilon_{ij})\delta(-y)\ , \tag{2.5}$$

$$\delta\mu_{ij}=\zeta(x,z)(\delta_{ij}-\mu_{ij})\delta(-y)\ . \tag{2.6}$$

The electromagnetic fields are also written in a perturbation expansion. We denote the unperturbed fields by $\mathbf{H}^0$ and $\mathbf{E}^0$ with first-order corrections $\mathbf{H}^{sc}$ and $\mathbf{E}^{sc}$. We assume a time dependence for the fields of the form $\exp(-i\omega t)$. From Maxwell's equations we obtain a wave equation for $\mathbf{H}^{sc}$:

$$\nabla\times\overleftrightarrow{\epsilon}^{f\,-1}\nabla\times\mathbf{H}^{sc}-\omega_0^2\overleftrightarrow{\mu}^{f}\mathbf{H}^{sc}=\omega_0^2\delta\overleftrightarrow{\mu}\mathbf{H}_0-i\omega_0\nabla\times\overleftrightarrow{\epsilon}^{f\,-1}\delta\overleftrightarrow{\epsilon}\mathbf{E}_0\ . \tag{2.7}$$

For the rest of the paper, $\omega_0=\omega/c$. An equivalent expression for (2.7) is

$$\epsilon_k^f\sum_{j,m}{}'\left[\frac{1}{\epsilon_m^f}\frac{\partial^2}{\partial x_j\partial x_k}-\delta_{jk}\left[\sum_l\frac{1}{\epsilon_m^f}\frac{\partial^2}{\partial x_1^2}\right]-\omega_0^2\mu_{kj}^f\right]H_j=F_k\ . \tag{2.8}$$

The prime on the sum means that $m\neq j,k,l$. Since the dielectric tensor is diagonal in this problem, we set $\epsilon_{kk}=\epsilon_k$.

The vector $\mathbf{F}$ represents the driving terms and is given by

$$F_k=\omega_0^2\epsilon_k^f\sum_j\delta\mu_{kj}H_j^0-i\omega_0\epsilon_k^f\sum_{j,l}e_{kjl}\frac{\partial}{\partial x_j}\left[\frac{\delta\epsilon_1}{\epsilon_1^f}E_1^0\right]\ . \tag{2.9}$$

Here e_{jkl} is the Levi-Civita tensor.

We solve the perturbed wave equation (2.8) through a Green's function method. The scattered field is determined by

$$H_j^{sc}=\sum_k\int d\mathbf{x}'g_{jk}(\mathbf{x},\mathbf{x}')F_k\ , \tag{2.10}$$

where g_{ij} is the ijth component of the semi-infinite antiferromagnetic Green's function tensor. The volume of integration is over all of space. We refer the reader to paper I for the derivation and explicit form of the g_{ij}.

We now limit ourselves, for reasons discussed in paper I, to the simpler case of propagation in the xy plane with the incident electric field in the z direction. In this case none of the quantities in (2.8) depend on z and we can Fourier transform in the x variable. The one-dimensional Fourier expansion for g_{ij} is

$$g_{ij}(\mathbf{x},\mathbf{x}')=\int_{-\infty}^{\infty}\frac{dk_x}{2\pi}e^{ik_x(x-x')}g_{ij}(k_x;y,y')\ . \tag{2.11}$$

The relevant quantities for the transform of $\mathbf{F}$ are $\mathbf{H}^0$ and ζ. We restrict ourselves to surface irregularities that depend only on the x coordinate and are independent of z. This restriction allows a reasonable description of gratings but is incapable of fully describing a randomly rough surface. To see this, suppose the roughness varied in the z direction. We would then expect some scattering into propagation directions in the z direction (parallel to the applied field). There would also be some scattering of the incident wave into other polarization states, i.e., the production of scattered waves with electric field components normal to the surface. In our simplified theory, we only consider incident and scattered waves which are polarized with their electric fields parallel to the z axis and which propagate in the xy plane. This theory can thus describe a grating with a variable period in the x direction (one-dimensional roughness), but not two-dimensional roughness.

The x-dependent surface profile function has the one-dimensional expansion

$$\zeta(x)=\int_{-\infty}^{\infty}\frac{dk_x}{2\pi}e^{-ik_xx}\zeta(k_x)\ . \tag{2.12}$$

Finally, the unperturbed fields have only one Fourier component:

$$H_i^0(\mathbf{x})=e^{ik_{x0}x}H_i^0(k_{x0},y')\ , \tag{2.13}$$

$$E_z^0(\mathbf{x})=e^{ik_{x0}x}E_z^0(k_{x0},y')\ . \tag{2.14}$$

k_{x0} is the wave vector of the unperturbed wave. In our problem, the unperturbed field originates from a traveling electromagnetic wave incident on the rough surface of the antiferromagnet. The amplitude of the unperturbed fields in (2.13) and (2.14) then depends on k_{x0} and is determined in each region of space by the appropriate Fresnel relations. The pertinent formulas are presented in the Appendix.

Using the transforms (2.11–2.14), the scattered field of (2.10) can be written in the compact notation

$$\mathbf{H}^{sc}(\mathbf{x})=\frac{1}{4\pi^2}\int_{-\infty}^{\infty}dk_x\mathbf{\Lambda}(k_x,y)\zeta(k_x-k_{x0})e^{ik_xx}\ , \tag{2.15}$$

where the components of the vector $\mathbf{\Lambda}$ are defined by

$$\Lambda_x = \int_{-\infty}^{\infty} dy' \delta(-y') \left[\omega_0^2[(1-\mu_2)H_x^0(k_{x0},y') - i\mu_2 H_y^0(k_{x0},y')] + iE_z^0 \frac{\omega_0}{\epsilon_z^f}(1-\epsilon_2)\frac{\partial}{\partial y'} \right] \epsilon_z^f g_{xx}(k_x;y,y')$$
$$+ \int_{-\infty}^{\infty} dy' \delta(-y') \left[\omega_0^2[(1-\mu_2)H_y^0(k_{x0},y') + i\mu_2 H_x^0(k_{x0},y')] + iE_z^0 \frac{\omega_0}{\epsilon_z^f}(1-\epsilon_2)\frac{\partial}{\partial y'} \right] \epsilon_z^f g_{xy}(k_x;y,y') \quad (2.16)$$

and

$$\Lambda_y = \int_{-\infty}^{\infty} dy' \delta(-y') \left[\omega_0^2[(1-\mu_2)H_x^0(k_{x0},y') - i\mu_2 H_y^0(k_{x0},y')] + iE_z^0 \frac{\omega_0}{\epsilon_z^f}(1-\epsilon_2)\frac{\partial}{\partial y'} \right] \epsilon_z^f g_{yx}(k_x;y,y')$$
$$+ \int_{-\infty}^{\infty} dy' \delta(-y') \left[\omega_0^2[(1-\mu_2)H_y^0(k_{x0},y') + i\mu_2 H_x^0(k_{x0},y')] + iE_z^0 \frac{\omega_0}{\epsilon_z^f}(1-\epsilon_2)\frac{\partial}{\partial y'} \right] \epsilon_z^f g_{yy}(k_x;y,y') \, . \quad (2.17)$$

In deriving these formulas an integration by parts has been done, shifting the derivatives off of $\delta\overleftrightarrow{\epsilon}\mathbf{E}$ and onto the Green's functions.

As noted by Mills and Maradudin[1] and others,[12] the evaluation of the integrals in (2.16) and (2.17) is not obvious since the discontinuity of the integrand allows for a number of possible solutions. Following Mills,[2] we take a prescription which is consistent with previous perturbative treatments.[8] This prescription makes the source of the scattered fields proportional to the amplitude of the unperturbed fields inside the material but located in vacuum just outside they $y=0$ plane. Hence we use the Green's functions appropriate for sources in the $y<0$ space with the driving fields (defined by 2.9) appropriate to the $y>0$ space.

These choices result in the following expressions for $\mathbf{\Lambda}$:

$$\Lambda_x = \epsilon_2 \left[\omega_0^2[(1-\mu_1)H_x^0(k_{x0},+) - i\mu_2 H_y^0(k_{x0},+')] + iE_z^0 \frac{\omega_0}{\epsilon_2}(1-\epsilon_2)\frac{\partial}{\partial y} \right] g_{xx}(k_x;y,-)$$
$$+ \epsilon_2 \left[\omega_0^2[(1-\mu_1)H_y^0(k_{x0},+) + i\mu_2 H_x^0(k_{x0},+')] + iE_z^0 \frac{\omega_0}{\epsilon_2}(1-\epsilon_2)k_x \right] g_{xy}(k_x;y,-) \quad (2.18)$$

and

$$\Lambda_y = \epsilon_2 \left[\omega_0^2[(1-\mu_1)H_x^0(k_{x0},+) - i\mu_2 H_y^0(k_{x0},+)] + iE_z^0 \frac{\omega_0}{\epsilon_2}(1-\epsilon_2)\frac{\partial}{\partial y} \right] g_{yx}(k_x;y,-)$$
$$+ \epsilon_2 \left[\omega_0^2[(1-\mu_1)H_y^0(k_{x0},+) + i\mu_2 H_x^0(k_{x0},+)] + iE_z^0 \frac{\omega_0}{\epsilon_2}(1-\epsilon_2)k_x \right] g_{yy}(k_x;y,-) \, . \quad (2.19)$$

The fields and Green's functions are evaluated at the flat surface, the $\pm$ signs indicating to which side of $y'=0$ the expressions belong. The derivatives, of course, are evaluated before the limiting process.

We can now calculate the energy flow in the scattered fields. The time-averaged Poynting vector is

$$\mathbf{S} = (c/4\pi)\mathbf{E}^{sc} \times \mathbf{H}^{sc*} \, . \quad (2.20)$$

We require one further notational device. So far in the discussion it has not been necessary to introduce a separate notation for fields in the material ($y>0$) and for fields outside the material ($y<0$). Since the Green's functions and wave vectors for $y>0$ are different than those for $y<0$, the explicit forms for $\mathbf{\Lambda}$, $\mathbf{E}^{sc}$, $\mathbf{H}^{sc}$, and $\mathbf{S}$ will also differ depending on whether they are taken in the material or outside of it. For the rest of the paper then, the subscript "$>$" will indicate that an expression is valid inside the material and "$<$" will indicate that an expression is valid outside the material (in vacuum). To reduce the number of equations which follow, we also define $\overleftrightarrow{\epsilon}_> = \overleftrightarrow{\epsilon}$ and $\overleftrightarrow{\epsilon}_< = \overleftrightarrow{1}$.

Away from the rough surface, the perturbed fields satisfy

$$\omega_0 \overleftrightarrow{\epsilon}_{\gtrless} \mathbf{E}_{\gtrless}^{sc} = -\mathbf{k}_{\gtrless} \times \mathbf{H}_{\gtrless}^{sc} \, , \quad (2.21)$$

where the "$\gtrless$" indicates that one must choose either the expression appropriate to the $y<0$ or the $y>0$ region. For the perturbed electric fields, we write

$$\mathbf{E}_{\gtrless}^{sc} = -\frac{1}{4\pi^2\omega_0} \overleftrightarrow{\epsilon}_{\gtrless}^{-1} \int_{-\infty}^{\infty} dk_x \mathbf{k}_{\gtrless} \times \mathbf{\Lambda}_{\gtrless}(k_x) \times \zeta(k_x - k_{x0}) e^{ik_x x} \, . \quad (2.22)$$

The wave vector inside the material is given by

$$\mathbf{k}_> = \hat{\mathbf{x}} k_x + \hat{\mathbf{y}} k_{y>} \, , \quad (2.23)$$

where the normal component, k_y, is found through the dispersion relation

$$k_{y>} = + \left[\omega_0^2 \left[\frac{\mu_1^2 - \mu_2^2}{\mu_1} \right] \epsilon_2 - k_x^2 \right]^{1/2} \, . \quad (2.24)$$

This relation is derived by Camley and Mills[13] and can also be found by setting the determinant of the homogeneous equations of motions to zero. The vacuum wave vector outside the material, $\mathbf{k}_<$, is defined by

$$\mathbf{k}_< = \hat{\mathbf{x}} k_x + \hat{\mathbf{y}} k_{y<} , \tag{2.25}$$

with the normal component given by the free space dispersion

$$k_{y<} = -(\omega_0^2 - k_x^2)^{1/2} . \tag{2.26}$$

Note that in both (2.24) and (2.26) the signs on the radicals have been chosen so as to represent waves decaying exponentially away from the surface when the arguments of the radicals are real and negative.

Taking the product $\mathbf{E}^{sc} \times \mathbf{H}^{sc*}$, we define the related quantities

$$\mathbf{P}_{\gtrless}(k_x,y) = \frac{-c}{64\pi^5 \omega_0^2} \int_{-\infty}^{\infty} dk_x' [\overleftrightarrow{\epsilon}_{\gtrless}^{-1} \mathbf{k}_{\gtrless} \times \mathbf{\Lambda}_{\gtrless}(k_x,y)] \times \mathbf{\Lambda}_{\gtrless}^*(k_x',y) \zeta(k_x - k_{x0}) \zeta^*(k_x - k_{x0}') e^{ix(k_x - k_x')} . \tag{2.27}$$

The vector functions $\mathbf{P}_{\gtrless}(k_x,y)$ give the scattered power flow per unit area with wave-vector component parallel to the surface in a range $k_x, k_x + dk_x$, at a distance y away from the surface of the material. The scattered power flows are then given simply by

$$\mathbf{S}_{\gtrless}(y) = \int_{-\infty}^{\infty} dk_x \mathbf{P}_{\gtrless}(k_x,y) . \tag{2.28}$$

Since the scattered fields and power flows depend on y through a complex exponential term originating in the Green's functions, for further calculations it is useful to illustrate this dependence explicitly by writing

$$\mathbf{\Lambda}_{\gtrless}(k_x,y) = \boldsymbol{\lambda}_{\gtrless}(k_x) \exp(i k_{y\gtrless} y) . \tag{2.29}$$

A y independent portion of $\mathbf{P}_{\gtrless}$ is also of use and referred to as $\mathbf{p}_{\gtrless}$. The specific form of $\mathbf{p}_{\gtrless}$ depends on the profile function $\zeta(k_x)$, and for the present we only note that $\mathbf{P}_{\gtrless}$ will consist of terms of the form

$$\mathbf{p}_{\gtrless}(k_x) \exp\{-2|y| \mathrm{Im}[k_{y\gtrless}(k_x)]\} . \tag{2.30}$$

Only the real part of the Poynting vector of Eq. (2.28) is useful in determining energy losses. Consequently, in the calculations which follow, it is to be understood that only the real part of $\mathbf{p}_{\gtrless}$ is used.

We now consider the question of how to represent the power lost from the specularly reflected beam. First, we normalize the Poynting vectors (2.28) to the illuminated surface area by dividing $\mathbf{p}$ by

$$P_0 = L_x L_z (c/4\pi) H^{(i)2} \cos\theta_0 . \tag{2.31}$$

$H^{(i)}$ is the amplitude of the unperturbed *incident* field, L_x is the width in x of the area illuminated by the incident beam and L_z is the width in z. θ_0 is the angle of incidence defined in Fig. 1.

We integrate the normalized expressions over an appropriate surface to obtain the net scattered energy flow per unit surface area. First we consider the vacuum energy flows. We begin by separating the k_x integral into integrals over two different regions. In the region $|k_x| < |\mathbf{k}_<|$ the integral describes the flow of energy in radiative states. Defining this flow as $I^r_<$, we have

$$I^r_< = \int d\mathbf{a} \cdot \int_{k_x < |\mathbf{k}_<|} dk_x \frac{\mathbf{p}_<(k_x)}{P_0} \exp[-2y \mathrm{Im}(k_{y<})] . \tag{2.32}$$

The surface of integration for the radiative integral is a cylinder of radius $L_x/2$ and length L_z whose axis coincides with the z axis of our geometry. In the vacuum region, $k_{y<}$ is pure real for the radiated energy and the integral is straightforward:

$$I^r_< = \frac{L_x L_z}{P} \int_{k_x^0 < |\mathbf{k}_<|} dk_x \hat{\mathbf{y}} \cdot \mathbf{p}_<(k_x) . \tag{2.33}$$

In the region $|k_x| > |\mathbf{k}_<|$ the integral describes the blow of energy in evanescent states. Calling this $I^e_<$, we have

$$I^e_< = \int d\mathbf{a} \cdot \int_{|k_x| > |\mathbf{k}_<|} dk_x \frac{\mathbf{p}_<(k_x)}{P_0} \exp[2y \mathrm{Im}(k_{y<})] . \tag{2.34}$$

The energy flow in the evanescent fields is parallel to the surface in the $\pm x$ direction, so the surface integral is over a strip of width L_z that extends from $y=0$ to $y=\infty$. Since $k_{y<}$ is pure imaginary for all k_x in this wave-vector region, the surface integral is easily performed with the result

$$I^e_< = \frac{L_z}{P} \int_{|k_x^0| > |\mathbf{k}_<|} dk_x \frac{\hat{\mathbf{x}} \cdot \mathbf{p}_<(k_x)}{2|\mathrm{Im}(k_{y<})|} . \tag{2.35}$$

In the material, $k_{y>}$ may be complex if damping exists. For the half cylinder region within the material, the imaginary part of k_y in the radiative integral is due solely to damping and represents an exponential decay of the wave into the material. If we assume that the width of the illuminating beam, L_x, is much smaller than the decay length then the surface integral in the material is done exactly as in the vacuum case:

$$I^r_> = \frac{L_x L_z}{P} \int_{k_x^0 < |\mathbf{k}_>|} dk_x \hat{\mathbf{y}} \cdot \mathbf{p}_>(k_x) . \tag{2.36}$$

The evanescent flows in the material are found in the same manner as in the vacuum case (except with the limits of integration over y from 0 to $-\infty$) with the result

$$I^e_> = \frac{L_z}{P} \int_{|k_x^0| > |\mathbf{k}_>|} dk_x \frac{\hat{\mathbf{x}} \cdot \mathbf{p}_>(k_x)}{2|\mathrm{Im}(k_{y>})|} . \tag{2.37}$$

Our ultimate goal is to calculate the change in reflectance due to the surface roughness. First we define

the sums $I_> = |I^e_>| + |I^r_>|$ and $I_< = |I^e_<| + |I^r_<|$. It is important to note that while $I_>$ and $I_<$ represent scattering into states inside and outside the material respectively, they do not by themselves determine the fraction of power scattered out of the specularly reflected beam. The most we can say is that if ΔR and ΔT represent the changes in reflectance and transmittance due to roughness induced scattering, then

$$(I_> + I_<)_{ns} = \Delta R + \Delta T \ . \tag{2.38}$$

Since we are interested in losses from the specular beams, we include only the nonspecular portions of the scattering ratios in (2.38). This is emphasized by the subscript ns.

We can approximate ΔR by first writing

$$\Delta R = (I_> + I_<)_{ns}/(1 + \Delta T/\Delta R) \tag{2.39}$$

and assuming that the perturbing roughness does not have an appreciable effect on the ratio of transmitted flux to reflected flux. We then have the approximation

$$\Delta T/\Delta R = T/R \ , \tag{2.40}$$

where T and R are the unperturbed transmittance and reflectance. This approximation can be viewed as an expansion of $\Delta T/\Delta R$ about $\zeta = 0$ where only the zeroth-order term, T/R, is kept. The change in reflectance due to surface roughness is then

$$\Delta R = (I_> + I_<)_{ns}/(1 + T/R) \ . \tag{2.41}$$

The ration T/R is calculated in the Appendix.

This argument can be stated another way. Suppose a surface is illuminated by light of intensity I. Next, define a transmitted energy t and a reflected energy r such that $T = t/I$ and $R = r/I$. When the surface is perfectly smooth, all of the incident energy appears in transmitted and reflected fields according to the ratios T and R. A rough surface, however, takes some of the incident energy and redistributes it into scattered fields according to the ratio $(I_> + I_<)_{ns}$. Let $\mathcal{E}$ be the intensity of the nonspecular scattered light before being normalized to the intensity of the incident light so that $\mathcal{E}/I = (I_> + I_<)_{ns}$. Calling the change in reflectance $\Delta R = \Delta r/I$ and the change in transmittance $\Delta T = \Delta t/I$, conservation of energy requires

$$r - \Delta r + t - \Delta t + \mathcal{E} = I \ . \tag{2.42}$$

As in (2.38) we write $\Delta r + \Delta t = \mathcal{E}$. Equation (2.42) can then be written

$$r + t + \mathcal{E} = I + \mathcal{E} \ . \tag{2.43}$$

We now normalize both sides of (2.43) to $I + \mathcal{E}$. With $\mathcal{E}$ small compared to I, the resulting terms can be expanded in $\mathcal{E}/I$. Keeping first-order terms, we have

$$R(1 - \mathcal{E}/I) + T(1 - \mathcal{E}/I) + \mathcal{E}/I = 1 \ . \tag{2.44}$$

In this approximation the reflectance and the transmittance are both reduced by the fraction $\mathcal{E}/I$, and we make the identification

$$\Delta R = R\,\mathcal{E}/I \ . \tag{2.45}$$

Using $I = t + r$, $T = t/I$, $R = t/I$, and $(I_> + I_<)_{ns} = \mathcal{E}/I$, this is equivalent to (2.41). The assumption that the surface roughness does not significantly change the ratio T/R is thus consistent with a first-order perturbation of the reflected and transmitted energies.

III. THE ONE-DIMENSIONAL GRATING

We now wish to evaluate the power scattered by a periodic, sinusoidal grating ingrained upon the surface of the antiferromagnet. The surface profile function for this case takes the form

$$\zeta(x) = h[\cos(sx) - 1]/2 \ . \tag{3.1}$$

The grating depth is given by h, which is assumed small in comparison to the incident wave's wavelength. The spatial period of the grating is $1/s$. Note that the expression for the grating is such that $\zeta(x) < 0$, as required by our evaluation of the integral in Eqs. (2.16) and (2.17).

Transforming, as per Eq. (2.12), we have

$$\zeta(k) = h[\delta(k - s) + \delta(k + s) - \tfrac{1}{2}\delta(k)] \ . \tag{3.2}$$

When substituted into the expressions for $\mathbf{S}$ given by (2.28), the delta functions pick out the Fourier coefficients of the scattered power flow corresponding to $k_{x0} + s$, $k_{x0} - s$, and k_{x0} from the integrals over k_x and k'_x. These terms correspond to the zero-order reflected beam plus the first-order diffracted beams. When evaluating the expressions for $\mathbf{p}_{\gtrless}$, however, one encounters terms proportional to $\exp(2isx)$ and $\exp(isx)$ which represent interference terms between the three beams. If we illuminate a large portion of the grating, we effectively average the scattered beams over a large range of x. Performing this spatial average, the interference terms vanish.

Substituting the profile function (3.2) into Eq. (2.28) we arrive at the following expressions for the power flow into the material:

$$\begin{aligned}\langle \mathbf{S}_> \rangle = \frac{-h^2}{64\pi^5\omega_0^2}\{&[\overleftrightarrow{\epsilon}_>^{-1}\mathbf{k}_>(k_{x0}+s)\times\boldsymbol{\lambda}_>(k_{x0}+s)]\times\boldsymbol{\lambda}^*_>(k_{x0}+s)\exp[-2y|\mathrm{Im}(k^+_{y>})|] \\ &+[\overleftrightarrow{\epsilon}_>^{-1}\mathbf{k}_>(k_{x0}-s)\times\boldsymbol{\lambda}_>(k_{x0}-s)]\times\boldsymbol{\lambda}^*_>(k_{x0}-s)\exp[-2y|\mathrm{Im}(k^-_{y>})|] \\ &+\tfrac{1}{4}[\overleftrightarrow{\epsilon}_>^{-1}\mathbf{k}_>(k_{x0})\times\boldsymbol{\lambda}_>(k_{x0})]\times\boldsymbol{\lambda}^*_>(k_{x0})\exp[-2y|\mathrm{Im}(k^0_{y>})|]\} \ .\end{aligned} \tag{3.3}$$

Here we have introduced the abbreviations $k^{\pm}_{y>} = k_{y>}(k_{x0} \pm s)$ and $k^0_{y>} = k_{y>}(k_{x0})$. The functional form for $k_{y>}$ is given explicitly by Eq. (2.26).

The brackets around $\mathbf{S}_{\gtrless}$ indicate that the expression is averaged over x with the assumption that L_x is much larger than $1/s$. Outside the material, we have the expression

$$\langle \mathbf{S}_< \rangle = \frac{-ch^2}{64\pi^5\omega_0^2}\{[\mathbf{k}_<(k_{x0}+s)\times\boldsymbol{\lambda}_<(k_{x0}+s)]\times\boldsymbol{\lambda}_<^*(k_{x0}+s)\exp[2y|\mathrm{Im}(k_{y<}^+)|]$$
$$+[\mathbf{k}_<(k_{x0}-s)\times\boldsymbol{\lambda}_<(k_{x0}-s)]\times\boldsymbol{\lambda}_<^*(k_{x0}-s)\exp[2y|\mathrm{Im}(k_{y<}^-)|]$$
$$+\tfrac{1}{4}[\mathbf{k}_<(k_{x0})\times\boldsymbol{\lambda}_<(k_{x0})]\times\boldsymbol{\lambda}_<^*(k_{x0})\exp[2y|\mathrm{Im}(k_{y<}^0)|]\} \ . \tag{3.4}$$

The k_x dependence of $k_{y<}$ is given by Eq. (2.28) and is abbreviated in the same manner as in (3.3).

Several comments are in order. First, we interpret these expressions as representing power flow due to sources originating in the surface grating. These sources are driven by the incident fields. When the surface roughness is "turned off," the scattered fields must vanish. This obviously holds for the scattered power flows of (3.3) and (3.4).

When the surface roughness is "turned on," some of the incident energy is scattered out of the specularly reflected beam. This is clearly represented by the first two terms in (3.3) and (3.4), which describe scattering into the first-order diffracted beams. Inclusion of higher-order perturbation terms in the wave equation (2.7) for the scattered fields would result in the appearance of higher-order diffracted beams in the power flow expressions.

The surface roughness does not necessarily scatter the incident energy in nonspecular directions, however. The third terms in Eqs. (3.3) and (3.4) represent scattering into the zeroth-order diffracted beam. These describe power flow scattered in the direction of the unperturbed specular beams.

For certain values of $k_{x0}\pm s$, $k_{y<}$ will be pure imaginary and will thus describe fields exponentially decaying away from the surface. These fields correspond to evanescent waves traveling along the surface perpendicular to the easy axis. Whether $k_{y<}$ is real or imaginary depends on the magnitude of k_{x0} (which depends on the angle of incident wave with respect to the surface) and the magnitude of the grating period $1/s$.

When the grating induces evanescent waves traveling along the surface, there exist frequencies where surface-polariton modes can be excited. In this way the grating allows for coupling between the incident electromagnetic wave and surface antiferromagnetic polaritons. To illustrate this, in Fig. 2 we reproduce dispersion curves for bulk and surface polaritons.[13] In this example and the rest that follow, the material is MnF_2, a uniaxial antiferromagnet with the parameters $H_e=7.87$ kG, $H_a=550$ kG, $M_s=0.6$ kG, and $\epsilon_2=5.5$. The antiferromagnetic resonance frequency Ω is given by $\Omega=\gamma(2H_aH_e+H_a^2)^{1/2}$, where γ is the gyromagnetic ratio. Unless otherwise stated, damping is always present with the value $1/\Omega\tau=0.0002$. The unitless frequency and wave vector are given by ω/Ω and kc/Ω, respectively.

These curves in Fig. 2 are for zero applied field. The shaded areas represent bulk polariton modes and the dashed lines rising out of the lower bulk band are surface-polariton modes. The solid lines inside the bulk bands and above the surface modes are the leaky modes described in paper I. The dark vertical line is the light line where $\omega_0=k$. The two dotted vertical lines correspond to the grating induced wave numbers $k_{x0}\pm s$ for the case $k_{x0}c/\Omega=0.7$ and $s=0.5\ c/\Omega$. (In MnF_2, with an antiferromagnetic resonance frequency $\Omega=268$ GHz, this s is approximately 0.5 mm.) For these values, $k_{y<}$ is pure imaginary for the $+s$ case and the corresponding scattered fields decay exponentially away from the surface. The light line does not intersect any of the surface polariton modes, but for this choice of s, the grating induced line of $k_{x0}+s$ intersects a surface mode. The presence of the grating thus allows an incident electromagnetic wave to couple with polariton modes inaccessible when the surface is ideally smooth. Note that higher-order terms in the power flow expressions would result in more grating induced lines being drawn, and hence couplings to portions of the surface-polariton modes at even shorter wavelengths.

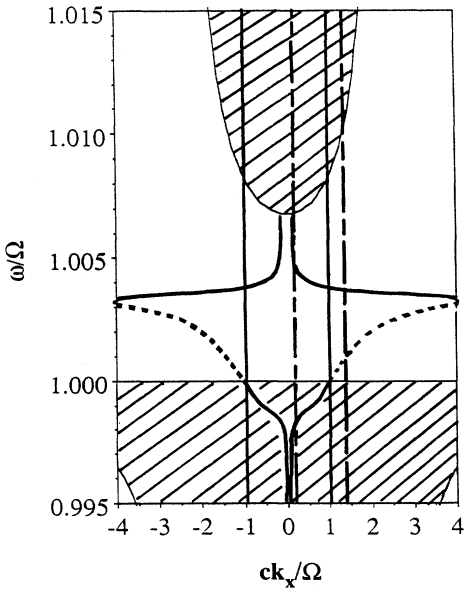

FIG. 2. Dispersion curve for antiferromagnetic polaritons, in MnF_2, with no applied field. The shaded areas are bulk bands and the dashed lines are surface modes. The solid lines are leaky modes. The dark vertical lines are light lines, where $\omega_0=k_x$. The dotted vertical lines are the grating induced lines, $q=k_x\pm s$, for $k_xc/\Omega=0.7$ and $s=0.5\ c/\Omega$.

The sum of the $+s$ and the $-s$ terms for the parallel power flows are plotted in Fig. 3 for $H_0=0$, $s=0.5\ c/\Omega$, and $\theta_0=45°$. We plot $\langle S_x^< \rangle/ch^2$ just outside the material in a vacuum at $y=0-$ and $\langle S_x^> \rangle/ch^2$ just inside the material at $y=0+$. The large peak at $\omega=1.001\ \Omega$ is approximately where the grating line intersects the surface mode shown in the dispersion curves of Fig. 2. Note that the energy flow outside the material is larger and oppositely directed to the energy flow inside the material. Inside the material, the susceptibilities are negative for the surface modes. In consequence, the Poynting vector is also negative and oppositely directed to the vacuum Poynting vector. This observation has also been made for surface plasmon-polaritons and surface magnetoelastic polaritons.

The smaller peak in Fig. 3 is from a surface resonance that lies *within* the bulk band. This peak corresponds to a location on the dispersion curve of Fig. 2 at $\omega=0.998\ \Omega$ on the $-s$ grating line. Note that this places the resonance on the left side of the light line, in a region where true surface polaritons cannot exist. These resonances are due to the Brewster-type leaky modes described in paper I.[14] A similar strong excitation of a leaky mode due to the coupling provided by a grating has been discussed earlier for the case of elastic waves by Glass and Maradudin.[15]

The leaky waves depend on material damping for their existence and so it is interesting to study them for larger damping parameters. In Fig. 4 we plot the parallel power flows for the same values of s and θ_0 as in Fig. 3 but with a larger damping constant of 0.0008. The quantity actually plotted is $\langle S_x \rangle/ch^2$. The larger peak is still the surface polariton but we see a distinct broadening of both the resonance and the polariton. In both Fig. 3 and 4 we also note the power flows inside the material are opposite those outside the material for both surface excitations. While the surface polariton carries most of its energy outside the material, the resonance carries most of its energy inside the material.

Having examined the possible energy flows inside and outside the material, we now look at the fraction of energy scattered out of an incident wave into these radiative and evanescent states. For the periodic grating the power ratio equations (2.33, 2.35, 2.36, and 2.37) become

$$I_>^r = \frac{h^2}{16H^{(i)2}\pi^4\omega_0^2\epsilon_2\cos(\theta_0)} \times[q\lambda_{y>}(q)-k_{y>}(q)\lambda_{x>}(q)]\lambda_{x>}^*(q)\ , \tag{3.5}$$

$$I_<^r = \frac{h^2}{16H^{(i)2}\pi^4\omega_0^2\cos(\theta_0)} \times[q\lambda_{y<}(q)-k_{y<}(q)\lambda_{x<}(q)]\lambda_{x<}^*(q)\ , \tag{3.6}$$

$$I_>^e = \frac{h^2}{32L_z|\mathrm{Im}[k_{y>}(q)]|H^{(i)2}\pi^4\omega_0^2\epsilon_2\cos(\theta_0)} \times[k_{y>}(q)\lambda_{x>}(q)-q\lambda_{y>}(q)]\lambda_{y>}^*(q)\ , \tag{3.7}$$

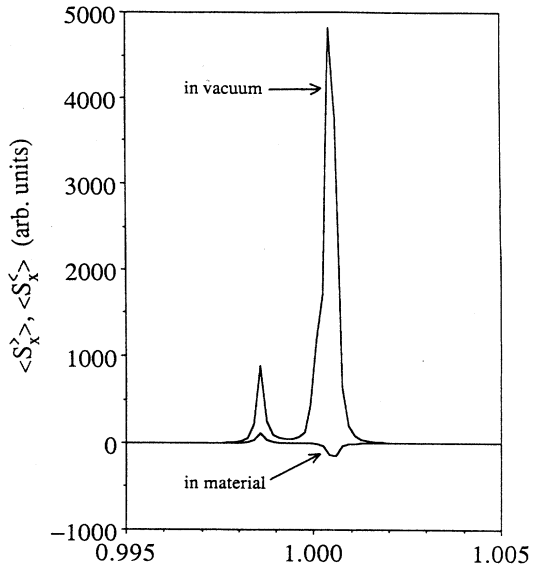

FIG. 3. Parallel power flows inside and outside the material as functions of frequency on a periodic grating with $s=0.5\ c/\Omega$. The quantities shown are proportional to $\langle S_x^> \rangle$ and $\langle S_x^< \rangle$. There is no applied field, $\theta_0=45°$, and damping is $1/\Omega\tau=0.0002$. The larger, higher frequency peak is due to a surface polariton. The other peak results from a surface resonance that lies within the bulk polariton band.

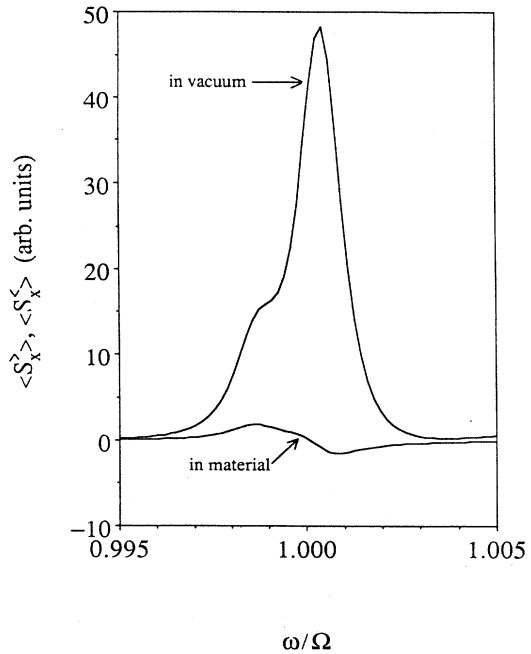

FIG. 4. Parallel power flows inside and outside the material as functions of frequency on a periodic grating with $s=0.5\ c/\Omega$. The quantities shown are proportional to $\langle S_x^> \rangle$ and $\langle S_x^< \rangle$. There is no applied field, $\theta_0=45°$, and damping is now $1/\Omega\tau=0.0008$. The peaks are much broader now than in the 0.0002 damping case of Fig. 3.

$$I^e_< = \frac{h^2}{32L_z|\mathrm{Im}[k_{y<}(q)]|H^{(i)2}\pi^4\omega_0^2\cos(\theta_0)} \times[k_{y<}(q)\lambda_{x<}(q)-q\lambda_{y<}(q)]\lambda^*_{y<}(q) \ . \quad (3.8)$$

Here q is understood as either k_{x0}, $k_{x0}+s$, or $k_{x0}-s$. As discussed earlier, the magnitude of q determines whether the power flow is radiative or evanescent. Thus $I^r_>$ represents radiative scattering in the material when $|q|<|\mathbf{k}_>|$ and $I^e_>$ represents evanescent scattering $|q|>|\mathbf{k}_>|$. Similarly, $I^r_<$ and $I^e_<$ represent radiative and evanescent scattering in vacuum when $|q|<|\mathbf{k}_<|$ and $|q|>|\mathbf{k}_<|$.

Before proceeding, we note that in an applied field the surface modes become highly nonreciprocal with respect to propagation direction [i.e., $\omega(+k_x)\neq\omega(-k_x)$]. For future reference, the dispersion curves for the bulk and surface polaritons in an applied field of 0.3 kG are presented in Fig. 5 for $1/\Omega\tau=0.0002$. The shaded areas are again bulk polariton bands and the dashed lines are surface-polariton modes. The solid lines are surface leaky modes.

Now it is possible, for certain choices of grating period s, to couple an incident wave whose parallel wave-vector component is in the $+x$ direction with surface modes whose wave vectors are in the $-x$ direction. For example, suppose a wave of frequency ω incident on a grating with period $1/s$ at some angle θ_0 couples to a surface mode traveling in the $-x$ direction with wave vector $k_{x0}-s$. It is also possible for an incident wave at another frequency ω' to couple with a surface mode traveling in the $+x$ direction with wave vector $k_{x0}'+s$ for the same angle of incidence. Thus for fixed s and θ_0, one can couple to both the $+k_x$ and the $-k_x$ polariton branches by scanning the frequency of the incident wave. Placing the material in applied field will increase the difference in frequencies by exploiting the nonreciprocity of the surface modes. An example is given in Fig. 6 where the evanescent power flows are plotted as functions of frequency for $s=3\ c/\Omega$, and $\theta_0=-45°$. An external field of 0.3 kG is applied. The quantities actually plotted are $I^e_> L_z/h^2$.

To identify the peaks in this figure, refer to the dispersion curves of Fig. 5 where we have sketched lines representing the grating induced wave vectors for $s=3\ c/\Omega$ and $k_{x0}c/\Omega=-0.7$. The peak nearest $\omega/\Omega=1$ in Fig. 6 corresponds to where the $-s$ grating line crosses the $-k_x$ surface-polariton mode in Fig. 6. The peak at $\omega=1.006\ \Omega$ in Fig. 6 corresponds to where the $+s$ grating line crosses the $+k_x$ surface polariton mode. The power flow for both modes is largest in vacuum and in the directions we would expect for the different modes: $I^e_<$ is positive for the $+k_x$ mode and negative for the $-k_x$ mode.

The two peaks labeled μ are at the antiferromagnetic resonance frequencies. At these frequencies μ_1 and μ_2 become very large and change sign. Since the driving fields

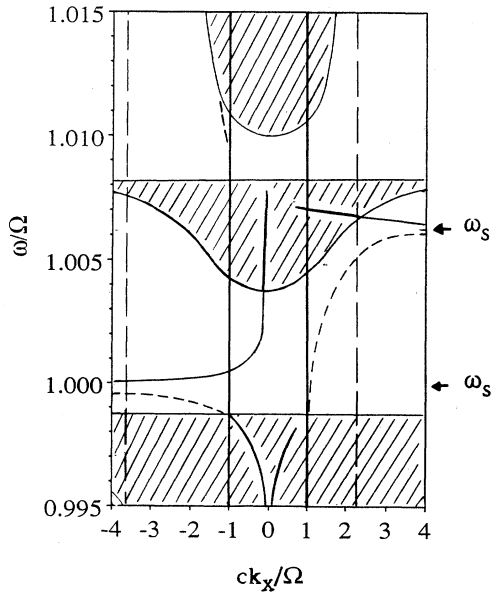

FIG. 5. Dispersion curve for antiferromagnetic polaritons, in MnF_2, with an applied field of 0.3 kG. The shaded areas are bulk bands and the dashed lines are surface modes. The solid lines are leaky surface modes. The dark vertical lines are the light lines, where $\omega_0=k_x$. The dotted vertical lines are the grating induced lines, $q=k_x\pm s$, for $k_xc/\Omega=-0.7$ and $s=3\ c/\Omega$. Note the strong nonreciprocity of the surface modes with respect to propagation direction.

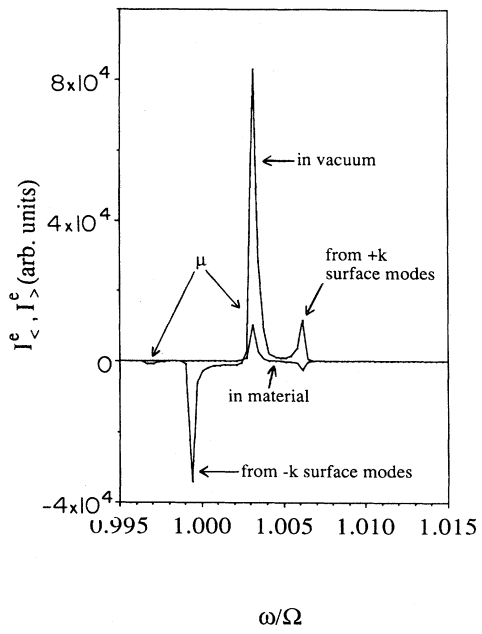

FIG. 6. Evanescent power flows inside and outside the material as functions of frequency on a periodic grating with $s=3\ c/\Omega$. The quantities shown are proportional to $I^e_>$ and $I^e_<$. The applied field is 0.3 kG, $\theta_0=-45°$, and damping is $1/\Omega\tau=0.0002$. For this s, we now pick up both the $+k_x$ surface mode and the $-k_x$ surface mode. The peaks labeled μ occur at frequencies where the susceptibilities become very large.

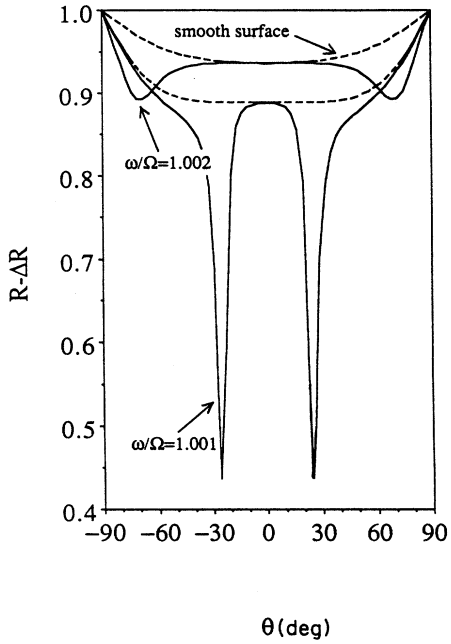

FIG. 7. Reflectivity as a function of θ_0 for a smooth surface (dashed lines) and a surface with a grating of period $s=1\ c/\Omega$ (solid lines). There is no applied field and damping is $1/\Omega\tau=0.0002$. The two frequencies couple with surface polaritons with different group velocities. The higher frequency polariton has a smaller group velocity and consequently has a greater density of k_x states. Thus it produces a broader and deeper reflectivity dip than the lower frequency mode.

of our perturbation expansion are proportional to μ_1 and μ_2, the theory breaks down at these frequencies. Thus the magnitude of the energy flow in the evanescent (and radiative) fields at these frequencies may be exaggerated with respect to the magnitude of the surface-polariton peaks.

In Fig. 7 the reflectance of the smooth surface R and the reflectance of the rough surface, $R-\Delta R$, is plotted versus θ_0 for two frequencies. There is no applied field and $s=1\ c/\Omega$. The grating height is $h=0.0002\ c/\Omega$ (for MnF_2, this height is approximately 0.2 μm) and the width of the illuminating beam L_x is set equal to Ω/c for convenience. We see that the presence of the grating introduces dips into the reflectance which are not seen for the smooth surface. These dips are, as usual, due to the coupling to surface polaritons, in this case the "true" surface polaritons, not the surface resonances. The dips are reciprocal in angle and are much further apart at the higher frequency than at the lower. This is due to the positive group velocity of the modes, as shown in Fig. 2, where the higher frequency modes exist at larger wave vectors. An interesting point is the increased width of the dips at the higher frequency. This is due to the group velocity, which decreases with increasing frequency, thus creating a higher density of states at the higher frequency. Since damping allows the incident wave to excite surface polaritons over a small range of frequency, a greater density of states allows the incident wave to excite a larger number of polariton states.

IV. RANDOM ROUGHNESS

The case of random roughness is somewhat simpler algebraically than the one-dimensional grating. We begin by calculating the average of S over the possible height profiles $\zeta(x)$. We assume a Gaussian form for the correlation function[1]

$$\langle \zeta(x)\zeta^*(x+x')\rangle = h^2 e^{-x^2/\sigma^2} . \tag{4.1}$$

Here h corresponds to the mean square height $\langle \zeta^2(x)\rangle$ and σ is the correlation length for the distribution of profiles. The Fourier transform is simply

$$\langle \zeta(k)\zeta^*(k')\rangle = \frac{1}{4\pi} h^2\sigma^2 \exp(-k^2\sigma^2/4)\delta(k-k') . \tag{4.2}$$

Using the profile correlation function of (4.2), the power ratio equations (2.33, 2.35, 2.36, and 2.37) are given by

$$I^r_> = \frac{h^2\sigma^2}{64H^{(i)2}\pi^5\omega_0^2\epsilon_2\cos(\theta_0)} \int_{-|\mathbf{k}_>|}^{|\mathbf{k}_>|} dk_x [k_x\lambda_{y>}(k_x) - k_{y>}\lambda_{x>}(k_x)]\lambda^*_{x>} \exp[-(k_x-k_{x0})^2\sigma^2/4] , \tag{4.3}$$

$$I^r_< = \frac{h^2\sigma^2}{64H^{(i)2}\pi^5\omega_0^2\cos(\theta_0)} \int_{-|\mathbf{k}_<|}^{|\mathbf{k}_<|} dk_x [k_x\lambda_{y<}(k_x) - k_{y<}\lambda_{x<}(k_x)]\lambda^*_{x<} \exp[-(k_x-k_{x0})^2\sigma^2/4] \tag{4.4}$$

for the radiative fields, and

$$I^e_> = \frac{h^2\sigma^2}{128L_xH^{(i)2}\pi^4\omega_0^2\epsilon_2\cos(\theta_0)} \int_{|k_x|>|\mathbf{k}_>|} dk_x [k_{y>}\lambda_{x>}(k_x) - k_x\lambda_{y>}(k_x)]\lambda^*_{y>}(k_x) \frac{\exp[-(k_x-k_{x0})^2\sigma^2/4]}{\mathrm{Im}(k_{y>})} , \tag{4.5}$$

$$I^e_< = \frac{h^2\sigma^2}{128L_xH^{(i)2}\pi^4\omega_0^2\cos(\theta_0)} \int_{|k_x|>|\mathbf{k}_<|} dk_x [k_{y<}\lambda_{x<}(k_x) - k_x\lambda_{y<}(k_x)]\lambda^*_{y<}(k_x) \frac{\exp[-(k_x-k_{x0})^2\sigma^2/4]}{\mathrm{Im}(k_{y<})} \tag{4.6}$$

for the evanescent fields.

The change in reflectivity is calculated by (2.41) as for the periodic grating. The nonspecular portions of $I^r_>$ and $I^r_<$ are calculated by excluding from the integration a small region about k_{x0}. This exclusion has a physical interpretation if we relate the Fourier amplitudes at each k_x to a scattering angle θ_s via the geometrical relation

$$k_x = |\mathbf{k}_>| \sin\theta_s \ . \tag{4.7}$$

In a reflection experiment, the excluded region would be the angular width of a detector. For our purposes we assume that this width is one degree and exclude from the integrations in Eqs. (4.3)-(4.6) the k_x values in the range $|\mathbf{k}_>|\sin(\theta_0+\frac{1}{2}°)$ to $|\mathbf{k}_>|\sin(\theta_0-\frac{1}{2}°)$.

With random roughness, we have an infinite collection of grating periods which produce an effective "width" in wavelength analogous to the damping width in frequency. This width is measured by the correlation length σ. Smaller values of σ lead to a greater smearing in wavelength while larger values indicate a smoother surface and a narrower wavelength range.

The dependence of the scattering on σ is shown in Figs. 8 and 9. In both figures $I^e_<$ is plotted as a function of frequency for $\theta_0 = -45$. There is an applied field of 0.3 kG. In Fig. 8, $\sigma = 0.1\ c/\Omega$ (for MnF_2, this correlation length is approximately 0.1 mm). The largest peak represents coupling with the $-k_x$ surface mode of Fig. 5.

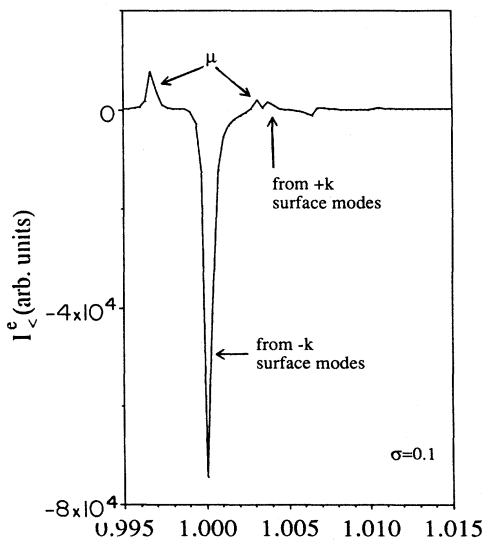

FIG. 8. Evanescent power flows outside the material as functions of frequency on a rough surface with $\sigma = 0.1\ c/\Omega$. The quantity shown in proportional to $I^e_<$. The applied field is 0.3 kG, $\theta_0 = -45°$, and damping is $1/\Omega\tau = 0.0002$. For this σ, we pick up both the $+k_x$ surface mode and the $-k_x$ surface mode near their limiting frequencies where the density of states is largest.

The largest coupling occurs where the density of states is the greatest. In Fig. 5 this occurs where the surface branches flatten out and the group velocity approaches zero. Since this occurs at rather large wave vectors, a fairly rough surface is required to allow coupling with an incident wave. The μ peaks discussed earlier are present, but dwarfed in comparison to the surface mode peak. We note that there is also a peak from the $+k_x$ branch, but this peak is very broad and its magnitude is small in comparison to the μ and $-k_x$ peaks.

In Fig. 9, $\sigma = 0.5\ c/\Omega$ (a correlation length of about 1 mm for MnF_2) and we notice a distinctly different profile for the scattered energy. There are now two distinct surface mode peaks and the smaller peak at the higher frequency represents coupling with the $+k_x$ surface mode. The magnitude of both surface mode peaks is considerably reduced in comparison to the μ peaks which are now clearly visible at $\omega_0/\Omega = 0.997$ and $\omega_0/\Omega = 1.003$. The surface mode peaks are also at lower frequencies than the rougher surface case. The shift in frequency and the reduced amplitudes of these surface mode peaks are due to lack of coupling to the higher (and denser) frequency portions of the surface mode dispersion curves. The strongest coupling for this smoother surface now occurs nearer to the light line.

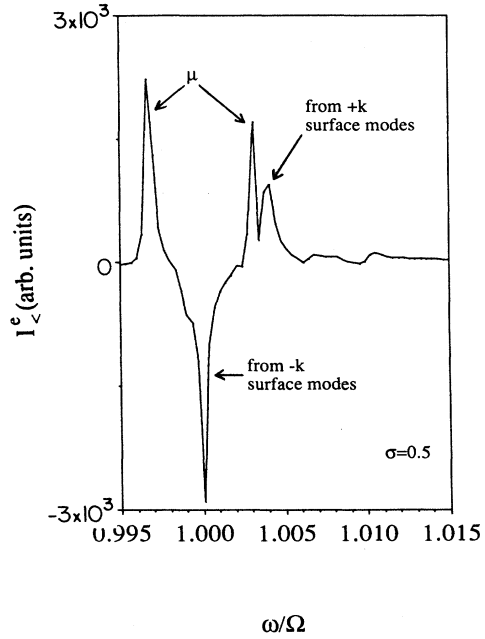

FIG. 9. Evanescent power flows outside the material as functions of frequency on a rough surface with $\sigma = 0.5\ c/\Omega$. The quantity shown is proportional to $I^e_<$. The applied field is 0.3 kG, $\theta_0 = -45°$, and damping is $1/\Omega\tau = 0.0002$. For this σ, we pick up contributions from the surface polaritons nearer the light line. These polaritons have relatively large group velocities and small state densities, hence they are not as strong scatters as the shorter wavelength polaritons. Note the prominence of the "μ" peaks compared to the surface-polariton peaks.

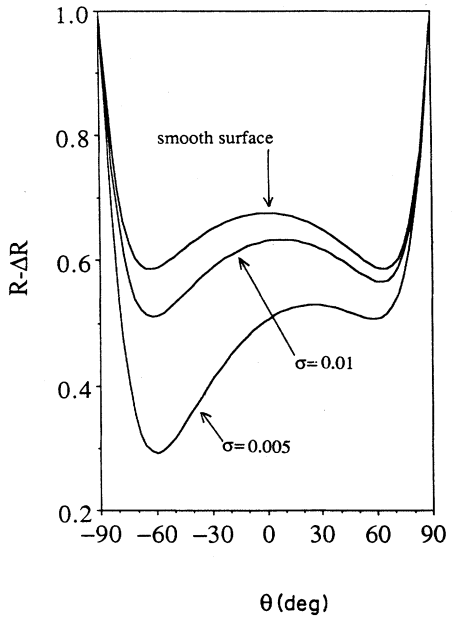

FIG. 10. Reflectivity as a function of θ_0 for a smooth surface, a rough surface with $\sigma=0.01\ c/\Omega$, and a rough surface with $\sigma=0.005\ c/\Omega$. There is an applied field of 0.3 kG and damping is $1/\Omega\tau=0.0002$. The root mean square height is $h=0.003\ c/\Omega$. The frequency of the incident wave is 0.9989 kG which allows coupling to both the $+k_x$ and the $-k_x$ surface polariton. With the applied field, these modes have different group velocities. The largest dip is due to the $+k_x$ surface polariton which has the greatest density of states nearest the light line. As roughness is increased, the nonreciprocal reflection losses become more pronounced.

In Fig. 10 we explore the effect of σ on a reflection measurement. Here we plot the reflectance of the smooth surface R and the reflectance of the rough surface $R-\Delta R$ as functions of θ_0 in an applied field of 0.3 kG. The frequency in 0.9989 Ω and so the incident wave can couple with both the $+k_x$ and the $-k_x$ surface mode branches of Fig. 5. The root-mean-square height is $h=0.003\ c/\Omega$ (a height of 30 μm for MnF_2) and the cases $\sigma=0.005\ c/\Omega$ and $\sigma=0.01\ c/\Omega$ are presented. First, we note that with this small damping value, the reflectance from the smooth surface is fairly reciprocal with respect to θ_0. The rough surface, however, induces nonreciprocity by coupling the incident wave more strongly with the surface-polariton modes.

The greatest losses occur for couplings with the $-k_x$ branch. This is because the $-k_x$ branch is flatter than the $+k_x$ branch, and thus has a greater density of states nearer the light line than the $+k_x$ branch. We also see that not only has the change in reflectivity increased with the slightly rougher surface, as expected by the σ^2 dependence of ΔR, but the + and − peaks are also more pronounced.

V. SUMMARY

We have applied the electromagnetic Green's functions for a semi-infinite antiferromagnet to a perturbative treatment of scattering from two types of surface roughness: a periodic grating and a surface with random roughness in one dimension. For certain choices of grating periods and incident angles, a periodic grating can induce coupling between incident electromagnetic waves and surface polaritons by creating evanescent fields that travel parallel to the surface of the material. The surface polaritons have a greater density of states at short wavelengths, and large grating periods can lead to stronger couplings by allowing the incident wave to interact with short wavelength surface polaritons.

When damping is present in the material, a grating can allow coupling to the leaky Brewster-type modes that may exist in frequency and wavelength regions forbidden to surface polaritons.

Random roughness creates a "width" in wavelength analogous to the width in frequency created by material damping. As the surface becomes rougher, the incident wave couples strongly to surface modes over a greater range of wavelengths. In a reflection experiment increased roughness may enhance nonreciprocal reflectivity changes by increasing the range of wavelengths over which the incident beam can couple with one of the surface mode branches.

ACKNOWLEDGMENTS

The work of R.L.S. was supported by the Air Force Office of Scientific Research, Bolling Air Force Base, Washington, D.C. The work of R.E.C. was supported by the Army Research Office under Contract No. DAAL03-88-K-0061.

APPENDIX: FRESNEL RELATIONS

The amplitudes of the driving fields in the material are written in terms of the incident wave's amplitude, $H^{(i)}$. The relations are derived in the usual manner by imposing Maxwell's continuity conditions on the unperturbed tangential $\mathbf{H}^0$ fields and the tangential $\mathbf{E}^0$ fields. Using

$$k_0^2=k_{x0}^2+k_{y0}^2=\omega_0^2 \tag{A1}$$

for the magnitude of the free space wave vector, and

$$k^2=k_{x0}^2+k_y^2=\epsilon_2\omega_0^2(\mu_1^2-\mu_2^2)/\mu_1 \tag{A2}$$

for the magnitude of the wave vector in the material, the amplitudes of the components of the transmitted wave are

$$H_x^0(k_x,y_0)=\frac{2\epsilon_2 k_0 k_{y0} k_y}{k^2 k_{y0}+\epsilon_2 k_0^2 k_y}H^{(i)}e^{iyk_y} \tag{A3}$$

for the x component, and

$$H_y^0(k_x,y_0)=\frac{-2\epsilon_2 k_0 k_{y0} k_{x0}}{k^2 k_{y0}+\epsilon_2 k_0^2 k_y}H^{(i)}e^{iyk_y} \tag{A4}$$

for the y component.

Finally, the ratio of the transmittance to the reflectance is found to be

$$\frac{T}{R}=\left[\frac{2\epsilon_2 k k_0 k_{y0}}{k^2 k_{y0}-\epsilon_2 k_0^2 k_y}\right]^2. \tag{A5}$$

[1]A. A. Maradudin and D. L. Mills, Phys. Rev. B **11**, 1892 (1975).
[2]D. L. Mills, Phys. Rev. B **12**, 4036 (1975).
[3]D. L. Mills, Phys. Rev. B **15**, 3097 (1977).
[4]A. A. Maradudin and W. Zierau, Phys. Rev. B **14**, 484 (1976).
[5]B. Laks, D. L. Mills, and A. A. Maradudin, Phys. Rev. B **23**, 4965 (1981).
[6]M. Weber and D. L. Mills, Phys. Rev. B **27**, 2698 (1983).
[7]S. Rice, Commun. Pure Appl. Math **14**, 351 (1951).
[8]E. Kruger and E. Kretshmann, Z. Phys. **237**, 1 (1970).
[9]J. M. Elson and R. H. Ritchie, Phys. Rev. B **4**, 4129 (1971).
[10]F. Toigo, A. Marvin, V. Celli, and N. R. Hill, Phys. Rev. B **15**, 5618 (1977).
[11]R. E. Camley, N. E. Glass, and A. A. Maradudin, J. Appl. Phys. **53**, 3170 (1982).
[12]G. S. Agarwal, Phys. Rev. B **14**, 846 (1976).
[13]R. E. Camley and D. L. Mills, Phys. Rev. B **26**, 1280 (1982).
[14]The sign on α was chosen such that the Green's functions could represent a leaky wave excitation, an approximation discussed in paper I.
[15]N. E. Glass and A. A. Maradudin, J. Appl. Phys. **54**, 796 (1983).